Hexagonal AlN: Dimensional-crossover-driven band-gap transition

C. Bacaksiz,[1,*] H. Sahin,[2] H. D. Ozaydin,[1] S. Horzum,[2] R. T. Senger,[1] and F. M. Peeters[2]
[1]*Department of Physics, Izmir Institute of Technology, 35430 Izmir, Turkey*
[2]*Department of Physics, University of Antwerp, 2610 Antwerp, Belgium*
(Received 5 November 2014; revised manuscript received 11 February 2015; published 27 February 2015)

Motivated by a recent experiment that reported the successful synthesis of hexagonal (h) AlN [Tsipas *et al.*, Appl. Phys. Lett. **103**, 251605 (2013)], we investigate structural, electronic, and vibrational properties of bulk, bilayer, and monolayer structures of h-AlN by using first-principles calculations. We show that the hexagonal phase of the bulk h-AlN is a stable direct-band-gap semiconductor. The calculated phonon spectrum displays a rigid-layer shear mode at 274 cm^{-1} and an E_g mode at 703 cm^{-1}, which are observable by Raman measurements. In addition, single-layer h-AlN is an indirect-band-gap semiconductor with a nonmagnetic ground state. For the bilayer structure, AA'-type stacking is found to be the most favorable one, and interlayer interaction is strong. While N-layered h-AlN is an indirect-band-gap semiconductor for $N = 1 - 9$, we predict that thicker structures ($N \geqslant 10$) have a direct band gap at the Γ point. The number-of-layer-dependent band-gap transitions in h-AlN is interesting in that it is significantly different from the indirect-to-direct crossover obtained in the transition-metal dichalcogenides.

DOI: 10.1103/PhysRevB.91.085430 PACS number(s): 81.05.ue, 68.47.Fg, 68.43.Bc, 68.43.Fg

I. INTRODUCTION

Bulk structures of III-V semiconductors have been widely studied due to their importance for technological applications such as blue light-emitting diodes, lasers operating in the blue and the ultraviolet regimes, high-temperature diodes, and transistors [1–6]. In addition, technological advances led to the emergence of novel low-dimensional forms of III-V binary compounds. Experimental fabrication of AlN nanowires [7–10], nanobelts [11–13], and nanodots [14,15] has already been reported. In recent years, theoretical and experimental studies of graphene [16] provided a wide range of knowledge for a new class of materials, and they opened up possibilities for the synthesis of many similar structures, such as silicene [17–20], germanene [20–23], transition-metal dichalcogenides (TMDs) [24–31], and hexagonal structures of III-V binary compounds (e.g., h-BN, h-AlN) [32–36]. Among the binary compounds, after single-layer BN, AlN is currently a material of much interest due to its semiconducting nature and its large band gap, which is suitable for device applications.

Following the first theoretical study on the stability of hexagonal AlN reported by Sahin *et al.* [36], successful experimental realization of hexagonal AlN phase was achieved very recently by Tsipas *et al.* [37]. In the early study of Du *et al.*, energetic and electronic properties of one-dimensional AlN nanostructures such as nanowires with hexagonal cross sections, double-and triple-walled faceted nanotubes, and single-walled faceted AlN nanotubes were investigated [38]. Between the first theoretical prediction and the experimental realization of h-AlN, other groups have also focused on this material. Zheng *et al.* [39] predicted that zigzag AlN nanoribbons have an indirect band gap whereas armchair AlN nanoribbons have a direct band gap, and these band gaps decrease monotonically with increasing ribbon width. Almeida *et al.* [40] studied the energetics and electronic properties of typical defects in an h-AlN network, such as vacancies, antisites, and impurities. It was shown that defects such as N vacancies and Si impurities lead to the breaking of the planar symmetry of the h-AlN sheet, as well as significant changes in the band structure in the vicinity of the Fermi level. In addition, Chen *et al.* systematically investigated the electronic structure of armchair and zigzag AlN, GaN nanoribbons, and also the electronic properties of AlN/GaN nanoribbon heterojunctions. They found that the band gap of both nanoribbons decreases monotonically as the ribbon widths increase, and that the band gap of the nanoribbon heterojunctions is closely related to the AlN/GaN ratio [41]. Shi *et al.* calculated the magnetic properties of undoped and transition-metal (TM) doped AlN nanosheets by using first-principles calculations. They reported that an AlN nanosheet is nonmagnetic, whereas a single $3d$ TM atom can bring about large local magnetic moments in TM-doped AlN nanosheets [42].

Motivated by the recent study of Tsipas *et al.* [37], who reported on the formation of stable h-AlN phases at the early stages of AlN growth, we aim to address the following experimental observations: (i) modification in electronic valence-band structure, (ii) a relatively large lattice parameter that was reported as an indication of the h phase, (iii) reduction in band gap in comparison with bulk wurtzite, and (iv) dynamical stability of h-AlN.

Our study reveals that the synthesized h-AlN, although it has structural similarities, electronically displays different characteristics from h-BN and TMDs. In addition to weak van der Waals (vdW) interactions, the ionic character of the interlayer interactions plays an important role in the electronic properties of mutilayered h-AlN. Therefore, while monolayers of h-BN and TMDs are direct-band-gap semiconductors, h-AlN has an indirect band gap. In addition, upon dimensional reduction from bulk to bilayer energy, the band gap decreases as was found for h-BN and TMDs.

The paper is organized as follows: In Sec. II we give details of our computational methodology. In Sec. III we provide a brief overview of the structural and electronic properties of hexagonal AlN (h-AlN) structure together with wurtzite structure. In Sec. IV the stability of few-layer structures

*cihanbacaksiz@iyte.edu.tr

and their electronic properties are investigated in detail. Our findings are discussed in Sec. V.

II. COMPUTATIONAL METHODOLOGY

Our investigations of the minimum energy configurations of different AlN structures and their electronic properties were carried out using the Vienna ab-initio simulation package VASP [43–46], which is based on density functional theory (DFT). The VASP code solves the Kohn-Sham equations [47] for a system with periodic boundary conditions using a plane-wave basis set iteratively. The Perdew-Burke-Ernzerhof (PBE) form of the generalized gradient approximation (GGA) [48,49] was adopted to describe electron exchange and correlation. The band-gap underestimation in bare GGA calculations is also examined by using the hybrid DFT-HSE06 functional [50]. The vdW interaction that is significant for layered h-AlN material was taken into account for all multilayer structures [51,52]. For the charge-transfer analysis, the Bader technique was used [53].

The kinetic energy cutoff of the plane-wave basis set was 500 eV in all calculations. The optimization of atomic positions was performed by minimizing the total energy and the forces on the atoms, hence the energy difference between sequential steps was taken to be 10^{-5} eV as a convergence criterion in the structural relaxation, and the convergence for the Hellmann-Feynman forces on each atom was taken to be 0.05 eV/Å. In addition, a Gaussian smearing factor of 0.05 eV was used for non-self-consistent calculations, and the pressures on the unit cell were decreased to a value less than 1.0 kB in all three directions. For the determination of accurate charge densities, Brillouin zone integration was performed using a $35 \times 35 \times 1$ Gamma centered mesh for the primitive unit cell. To avoid interaction between adjacent AlN monolayers and few-layer systems, our calculations were performed with a large unit cell including ∼14 Å vacuum space. We also calculated the cohesive energy (E_{coh}), which was formulated as $E_{\text{coh}} = (n_{\text{Al}}E_{\text{Al}} + n_{\text{N}}E_{\text{N}} - E_T)/(n_{\text{Al}} + n_{\text{N}})$, where E_T, E_{Al}, E_{N}, n_{Al}, and n_{N} are the total energy per unit cell, the energy of a free Al atom, the energy of a free N atom, and the number of Al and N atoms in a unit cell, respectively.

III. STRUCTURES OF BULK AlN

First we provide a brief overview of the characteristics of wurtzite and recently synthesized h-AlN before an extensive investigation of the number of layer-dependent properties of h-AlN is undertaken. At ambient conditions, AlN crystallizes in a wurtzite (wz) structure that belongs to the $P6_3mc$ space group. As shown in Table I, the PBE approximation gives the following structural parameters: $a = 3.11$ Å and $\frac{c}{a} = 1.61$. In the wz structure of AlN, each Al-N bond is formed by 2.35 e^- charge donation from an Al to a N atom, and therefore it has a highly ionic character. In parallel with the abundance of the wz form of AlN in nature, among the possible bulk structures, wz is the energetically most favorable one. The electronic dispersion shown in Fig. 1 indicates that wz-AlN is a semiconductor with a 4.2 eV direct band gap at the Γ point.

In addition to some early theoretical predictions [36], the stability of the hexagonal phase of AlN (h-AlN) was proven by a very recent experimental study [37]. Regarding the less layered structures or surfaces of wurtzite materials, transformation from wurtzite to a graphitelike structure that allows the removal of destabilizing dipoles is energetically more favorable [54]. This graphitelike hexagonal structure of AlN belongs to the $P6_3/mmc$ space group. The layered planar structure has two atoms in the unit cell, which has lattice vectors $\mathbf{v}_1 = a(\frac{1}{2}, \frac{\sqrt{3}}{2}, 0)$, $\mathbf{v}_2 = a(\frac{1}{2}, -\frac{\sqrt{3}}{2}, 0)$, and $\mathbf{v}_3 = c(0,0,1)$, where $|\mathbf{v}_1| = |\mathbf{v}_2|$. Atomic coordinates are $(\frac{|v_1|}{3}, \frac{|v_1|}{3}, 0)$ and $(\frac{2|v_1|}{3}, \frac{2|v_1|}{3}, 0)$ for the first and second type of atoms, respectively. We considered that the layers are AA' stacking (deciding the stacking of layers is explained in Sec. IIV B), which is shown in Fig. 1(b), and we found that the lattice constant is $a = 3.30$ Å and the distance between layers is $c = 2.08$ Å, which is smaller when compared to graphite and h-BN (∼3.33 and ∼3.30 Å for graphite [55,56] and h-BN [57–59], respectively). The intralayer atomic distance between Al and N atoms is 1.90 Å. This is the same as for wz-AlN. The cohesive energies are given in Table I.

As shown in Fig. 1(b), layered h-AlN is a direct-band-gap semiconductor that has a 3.4 eV band gap with band

TABLE I. Calculated lattice parameter in the lateral direction a and lattice parameter in the vertical direction c, the distance between layers d_{LL}, the intralayer atomic distance between Al and N atoms $d_{\text{Al-N}}$, the charge transfer from Al atom to N atom $\Delta\rho$, the cohesive energy E_{coh}, and the energy band gap of the structure E_{gap}. (d) and (i) indicate direct and indirect band gap, respectively.

	a (Å)	c (Å)	d_{LL} (Å)	$d_{\text{Al-N}}$ (Å)	$\Delta\rho$ (e)	E_{coh} (eV)	E_{gap} (eV)
Bulk wz-AlN	3.11	5.01		1.90	2.35	6.14	4.2 (d)
Bulk h-AlN	3.30	4.15	2.08	1.90	2.37	6.02	3.4 (d)
2L h-AlN	3.20		2.13	1.85	2.32	5.73	3.5 (i)
1L h-AlN	3.13			1.81	2.28	5.36	2.9 (i)

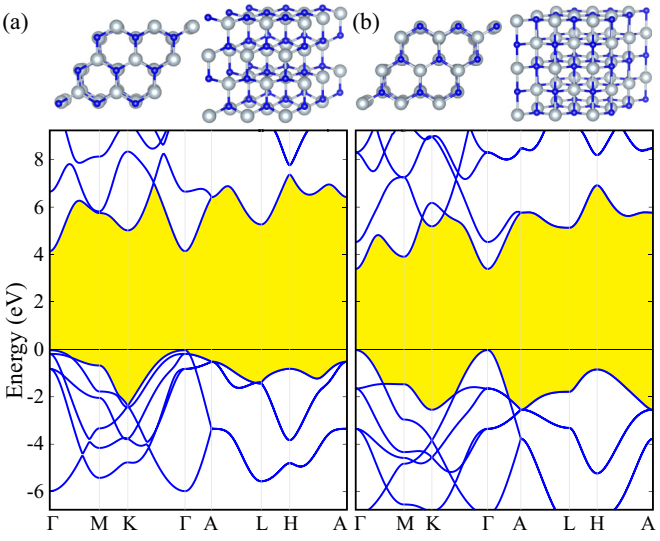

FIG. 1. (Color online) Top and tilted-side views of atomic structures of bulk (a) wurtzite and (b) hexagonal AlN (top panel), and their electronic band dispersion (lower panel).

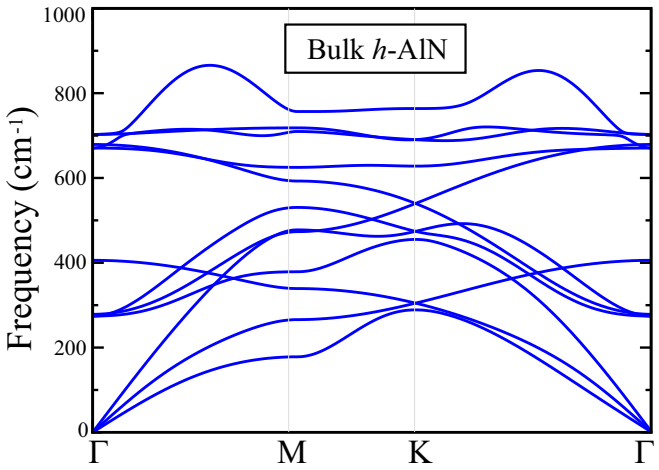

FIG. 2. (Color online) Phonon dispersion of bulk h-AlN.

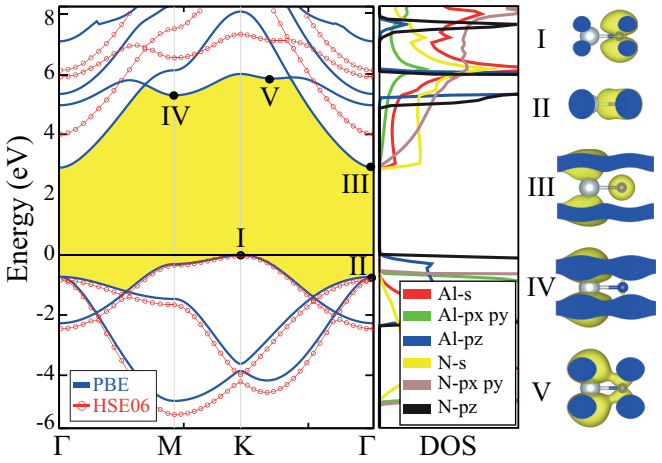

FIG. 3. (Color online) Monolayer h-AlN band diagram within PBE and HSE06 (left panel), partial density of states (middle panel), and the band decomposed charge densities of the band edges (right panel). Sections of 3D charge density that represent the connection to the neighboring cells are filled with blue color.

edges located at the Γ point. Therefore, our results confirm the experimentally reported band-gap reduction [37] in h-AlN compared to bulk wz-AlN. At the top of the VB, there is a single parabolic band for holes, and the main contributions are from the p_z orbital of N atoms. At the bottom of the CB, there is a single parabolic band and most of the states come from p_x orbitals of N atoms. Final charges of Al and N atoms are 0.63 e^- and 7.37 e^-, respectively. Therefore, 2.37 e^- charges are transferred from an Al to a N atom. The following section is devoted to understanding the characteristics of monolayer h-AlN and the nature of the interlayer interactions.

Lastly, we analyze the vibrational properties of the h-AlN phase by calculating the phonon spectrum in the whole Brillouin zone (BZ) using the small displacement methodology [60] for a 32-atomic supercell. As shown in Fig. 2, the phonon spectrum of h-AlN displays real eigenfrequencies in the whole BZ. Therefore, there is no doubt as to the dynamical stability of the h-AlN structure. Here we also see that differing from its h-BN counterpart, the optical and acoustical modes couple with each other at certain points in the BZ. In the case of h-AlN, there are four atoms per primitive unit cell and 12 phonon branches. The first three are acoustical phonon modes, while the phonon branch at 274 cm^{-1} is a doubly degenerate rigid layer shear mode, known as a low-energy E_g mode, involving the out-of-phase motion of atoms in adjacent planes. In addition, the highly dispersive phonon modes with eigenvalues 406 and 679 cm^{-1} at the zone center correspond to out-of-phase motion of Al and N atoms in adjacent layers. Interestingly, the contribution of the second atom type in these modes is negligibly small. The highest optical mode, doubly degenerate at the Γ point, has E_g symmetry and therefore it is expected to be measured in Raman experiments.

IV. MONOLAYER, BILAYER, AND FEW-LAYER h-AlN

A. Monolayer h-AlN

The first prediction of the dynamical stability and the electronic properties of single layers of h-AlN and similar III-V compounds were first reported by Sahin *et al.* [36]. Monolayer hexagonal structure belongs to the space group $P6_3/mmc$ with unit vectors $\mathbf{v}_1 = a(\frac{1}{2}, \frac{\sqrt{3}}{2}, 0)$, $\mathbf{v}_2 = a(\frac{1}{2}, -\frac{\sqrt{3}}{2}, 0)$, where $|\mathbf{v}_1| = |\mathbf{v}_2|$. In this configuration, the atomic coordinates are given as $(\frac{|v_1|}{3}, \frac{|v_1|}{3}, 0)$ and $(\frac{2|v_1|}{3}, \frac{2|v_1|}{3}, 0)$ for the first and second type of atoms, respectively. We calculated that the lattice constant of monolayer h-AlN is 3.13 Å and the distance between Al and N atoms is 1.81 Å, which is the lowest value when compared with bulk forms and bilayer structure as seen from Table I. These results are in good agreement with the measured lattice parameters (3.13 Å) of epitaxially grown of h-AlN, at early stages, by Tsipas *et al.* [37]. The cohesive energy of monolayer h-AlN is the lowest among the possible phases. It is also seen that the amount of charge transfer from Al to N decreases slightly from bulk to monolayer h-AlN.

Figure 3 illustrates the band diagrams, density of states, and also the 3D charge densities of states at the band edges for monolayer h-AlN. Differing from bulk h-AlN, which has a direct band gap at the Γ, the VBM of the monolayer is at the K point and the CBM is at the Γ point, therefore monolayer h-AlN is an indirect band-gap insulator with a 2.9 eV band gap. It is also seen that bare-GGA and DFT-HSE06 approximated electronic band dispersions shown in Fig. 3 are almost the same. With the DFT-HSE06 hybrid functional, h-AlN is an indirect-band-gap material with a band gap of 4.06 eV. It is also noteworthy to mention that h-BN is the counterpart of AlN with a direct band gap at the K point.

The right panel of Fig. 3 shows that the bonding states at VBM (label I) are mainly composed of N-p_z orbitals, and the degenerate state, with lower energy, at the Γ point (label II) stems from hybridized p_x and p_y orbitals. In addition, the CBM located at the Γ point has a quadraticlike dispersion (label III) and the relevant charge density is in the form of a surface state. Therefore, the conduction electrons in single-layer h-AlN display free-electron-like behavior. Moreover, the antibonding states with higher energy at the M and the K points are composed of mainly Al and a few N states together.

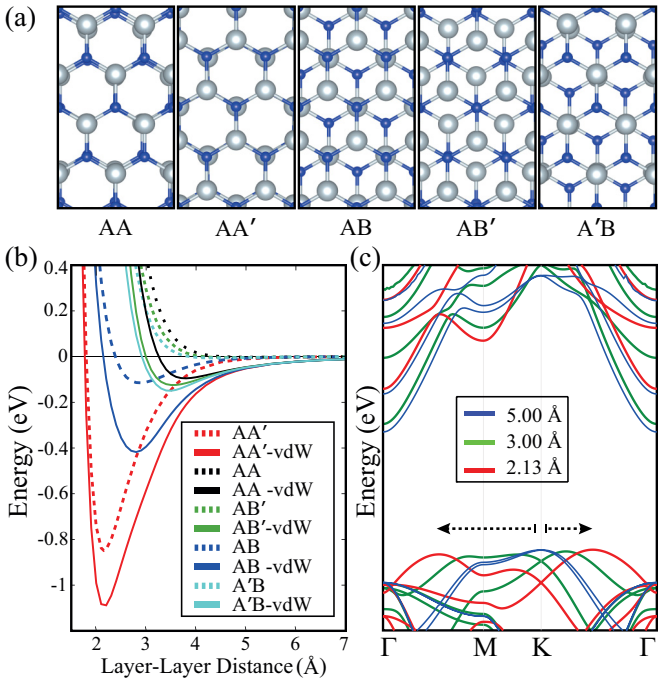

FIG. 4. (Color online) (a) Possible stackings between two layers of h-AlN. (b) Layer-layer interaction energy for different stackings. (c) Interlayer-spacing-dependent band dispersion of AA' stacked two layers of h-AlN.

B. Bilayer h-AlN and layer-layer interaction

During the growth of lamellar materials, prediction of the most preferable stacking sequence is of importance. To determine the stacking order of bilayer AlN, we examined five possible [see Fig. 4(a)] stacking types: AA (Al over Al and N over N), AA' (Al over N and N over Al), AB (Al over N and N over center of hexagon), $A'B$ (Al over Al and N over center of hexagon), and AB' (N over N and Al over center of hexagon).

To determine the interaction strength and interlayer interaction profile of the above-mentioned stacking orders of bilayer h-AlN, total energies were calculated as a function of layer-layer distance. As seen from Fig. 4(b), the largest interlayer coupling energy and shortest interlayer distance are obtained for AA'-type stacking. Therefore, AA' stacking corresponds to the ground-state stacking order. It is also seen that the vdW correction to the interaction energy is ∼250 meV per unit cell. In addition, for AA' stacking, layer-layer distance is 2.13 Å, which is the minimum value among all stacking combinations. Here it appears that due to the presence of surface states, the interlayer distance in bilayer h-AlN is slightly larger than that of bulk h-AlN. However, compared to graphite [55,56] and h-BN [57–59], and their bilayer forms, h-AlN has a smaller interlayer distance. The lattice parameter, 3.20 Å, which is the maximum value of all stacking combinations, differs slightly from the value obtained by self-correlation analysis of the experimental data (3.14 ± 0.06) for a few layers. This slight disagreement can be understood from the effect of the Ag(111) substrate.

Moreover, in Fig. 4(c), we analyze how the electronic band dispersion of an AA'-stacked bilayer is modified with varying interlayer distance. Negligibly interacting, weakly interacting, and highest interaction (ground-state) cases are illustrated using layer-layer distances of 5.00, 3.00, and 2.13 Å, respectively. The band diagram of the negligibly interacting case resembles the electronic structure of monolayer h-AlN. However, when the layers start to interact, for instance in the weakly interacting case [delineated by green lines in Fig. 4(c)], the top of the VBM is shifted toward the Γ zone center. When the interlayer distance reaches its optimum position, one of the VBMs appears at K-Γ while the other one is located at M-Γ. Interestingly, the location of the CBM in the BZ is independent from the interlayer distance. Hence from monolayer to bilayer, the indirect character is conserved and the band gap is changed from 2.9 to 3.5 eV.

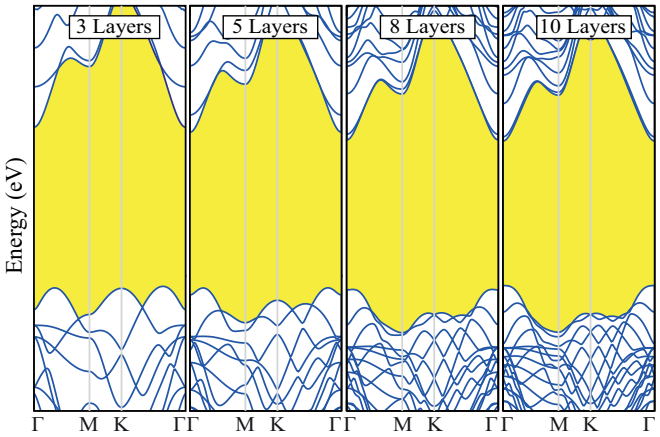

FIG. 5. (Color online) Evolution of electronic band dispersion of N-layer h-AlN.

C. Few-layer h-AlN

Synthesis of stable ultrathin h-AlN structures, submonolayer to 12 layers, was demonstrated recently by Tsipas *et al.* [37]. Our first-principles total energy optimization calculations revealed that the lamellar hexagonal structure of N-layered ($N = 1,2,\ldots$) AlN is a stable phase. As shown in Figs. 5 and 6, planarity of the few-layered structures is preserved, except the negligible buckling at the surface layers, while electronically few-layer h-AlN is significantly different from the monolayer one.

To illustrate how the electronic structure evolves with an increasing number of layers, we present the band dispersion of 3-, 5-, 8-, and 10-layered h-AlN in Fig. 5. Here there are several interesting trends that are worth noting: (i) the energy of the conduction-band edge at the K point decreases with an increasing number of layers, (ii) states at the conduction-band edge that have surface-state character remain unchanged. The energy difference between the band edges VBM (K) and CBM (Γ) increases from 2.92 eV for monolayer to 3.81 eV for 10-layer h-AlN, and (iii) the most significant influence of an additional number of layers is on the bonding states forming the valence-band maximum at the ΓM and the ΓK points. It appears that due to the strong interlayer interaction, each additional layer shifts these band edges toward the zone center. This gradual shift of VB edges continues up to 10 layers. Upon the formation of the 10th layer, the h-AlN

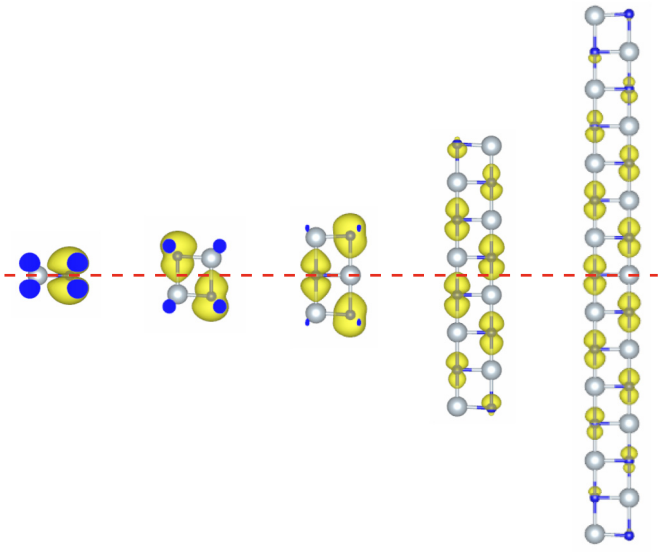

FIG. 6. (Color online) The evolution of the bonding charge density of h-AlN for monolayer, bilayer, 3-layer, 8-layer, and 15-layer. Sections of 3D charge density that represent the connection to the neighboring cells are filled with blue color.

structure reaches the bulk limit and it becomes a direct-band-gap semiconductor. Increasing the thickness further has no influence on the electronic properties of N-layered h-AlN, and they are direct-band-gap (3.22 eV for ten-layered) materials such as bulk h-AlN. As given in detail in Table II, transition energies between the points converge asymptotically to values of bulk h-AlN. Increasing the number of layers, cohesive energies converge to that of bulk h-AlN. It appears that only few-layer h-AlN structures with thickness $N \geqslant 10$ are suitable for lasing device applications. Here calculated modifications in electronic structure explain and support the experimental findings of Tsipas *et al.* [37].

However, the evolution of the VBM with a changing number of layers requires further attention. In Fig. 6 we present the 3D charge density of the electronic states located at the VBM. It is clearly seen that the character of the bonding state (VBM) is modified monotonically with an increasing number of layers. With an increasing number of layers, the hybridization between N-p_z states is weakened. In addition, due to the mild buckling, the interaction of the surface states that have sp^3-like character and N-p_z states vanishes in the vicinity of the upper- and lowermost layers. Therefore, for thick enough h-AlN materials, which are found to be larger than 10 layers, the electronic structure is mainly determined by uniformly distributed N-p_z states and hence the structure behaves like a bulk material having a direct band gap at the Γ symmetry point.

TABLE II. Calculated direct and indirect transition energies between the VB and CB edges of single- to 10-layered structures.

	$\Gamma \longrightarrow \Gamma$	$K \longrightarrow \Gamma$	$\Gamma M \longrightarrow \Gamma$	$K\Gamma \longrightarrow \Gamma$	E_{coh}
1L AlN	3.62	2.92			5.36
2L AlN	4.29		3.61	3.53	5.73
3L AlN	4.05	3.58	3.57	3.53	5.82
4L AlN	3.79		3.51	3.50	5.86
5L AlN	3.61	3.73	3.46	3.46	5.89
6L AlN	3.48		3.41	3.41	5.92
7L AlN	3.38	3.77	3.35	3.35	5.93
8L AlN	3.33		3.30	3.30	5.94
9L AlN	3.27	3.81	3.26	3.26	5.95
10L AlN	3.22				5.96

V. CONCLUSIONS

Using first-principles methodology, we investigated the thickness-dependent electronic properties of layered hexagonal AlN. First, we showed that the bulk structure of hexagonal AlN is a semiconductor with a direct band gap at the Γ point. Phonon spectrum analysis of this structure reveals two Raman-active modes at 274 and 703 cm^{-1}. Here, the lattice parameter of h-AlN, which is larger than the wurtzite phase, agrees with the experiment of Tsipas *et al.* [37] that reports the formation of hexagonal regions at the early stages of the growth process. Next, the formation of multilayer structures and the most favorable stacking order were investigated via total energy calculations. It is seen that, similar to the hexagonal BN counterpart, among the possible stackings, AA'-type stacking is the most favorable. It is worthwhile to note that the interlayer interaction is larger compared to similar layered materials with hexagonal lattice symmetry. Differing from some other two-dimensional crystal structures such as graphite, h-BN, and TMDs, here the ionic interlayer interaction is dominant between the h-AlN layers. Therefore, for the synthesis of h-AlN, the epitaxial growth technique performed by Tsipas *et al.* [37] appears more suitable than mechanical exfoliation.

Subsequently, the evolution of the electronic structure of N-layered h-AlN was investigated for structures with 1–15 layers. It is seen that unlike bulk h-AlN, monolayer h-AlN has an indirect band gap where VBM and CBM are at the K and the Γ points, respectively. Moreover, it is seen that upon the formation of additional layers, valence-band edges gradually shift toward the Brillouin zone center. Such a modification of the valence-band states is in good agreement with the experiment of Tsipas *et al.* [37]. It was also calculated that the few-layered structures reach the bulk limit and their electronic properties remain almost unchanged after the formation of 10 layers. Therefore, structures thicker than 10 layers exhibit a direct band gap of 3.22 eV at the Γ point. We believe that easy synthesis and the presence of a thickness-dependent band-gap crossover in few-layered hexagonal AlN structures are very important for novel device applications.

ACKNOWLEDGMENTS

This work was supported by the Flemish Science Foundation (FWO-Vl) and the Methusalem foundation of the Flemish government. Computational resources were provided by TUBITAK ULAKBIM, High Performance and Grid Computing Center (TR-Grid e-Infrastructure). C.B. and R.T.S. acknowledge the support from TUBITAK Project No 114F397. H.S. is supported by a FWO Pegasus Long Marie Curie Fellowship.

[1] C. Y. Yeh, Z. W. Lu, S. Froyen, and A. Zunger, Phys. Rev. B **45**, 12130 (1992).

[2] C. Y. Yeh, Z. W. Lu, S. Froyen, and A. Zunger, Phys. Rev. B **46**, 10086 (1992).

[3] H. Morkoc, S. Strite, G. B. Gao, M. E. Lim, B. Sverdlov, and M. Burns, J. Appl. Phys. **76**, 1363 (1994).

[4] I. Vurgaftman, J. R. Meyer, and L. R. Ram-Mohan, J. Appl. Phys. **89**, 5815 (2001).

[5] K. Miwa and A. Fukumoto, Phys. Rev. B **48**, 7897 (1993).

[6] N. E. Christensen and I. Gorczyca, Phys. Rev. B **50**, 4397 (1994).

[7] Q. Wu, Z. Hu, X. Z. Wang, Y. M. Hu, Y. J. Tian, and Y. Chen, Diamond Relat. Mater **13**, 38 (2004).

[8] J. H. Duan, S. G. Yang, H. W. Liu, J. F. Gong, H. B. Guang, X. N. Zhao, R. Zhang, and Y. W. Du, J. Phys. Chem. B **109**, 3701 (2005).

[9] Q. Zhao, H. Z. Zhang, X. Y. Xu, Z. Wang, J. Xu, D. P. Yu, G. H. Li, and F. H. Su, Appl. Phys. Lett. **86**, 193101 (2005).

[10] Y. Li, J. Xiang, F. Qian, S. Gradecak, Y. Wu, H. Yan, H. Yan, D. A. Blom, and C. M. Lieber, Nano Lett. **6**, 1468 (2006).

[11] Q. Wu, Z. Hu, X. Z. Wang, Y. Chen, and Y. Lu, J. Phys. Chem. B **107**, 9726 (2003).

[12] Y. B. Tang, H. T. Cong, F. Li, and H. M. Cheng, Diamond Relat. Mater. **16**, 537 (2007).

[13] L. S. Yu, Y. Y. Lv, X. L. Zhang, Y. Y. Zhang, R. Y. Zou, and F. Zhang, J. Cryst. Growth **334**, 57 (2011).

[14] W. H. Goh, G. Patriarche, P. L. Bonanno, S. Gautier, T. Moudakir, M. Abid, G. Orsal, A. A. Sirenko, Z. H. Cai, A. Martinez, A. Ramdane, L. Le Gratiet, D. Troadec, A. Soltani, and A. Ougazzaden, J. Cryst. Growth **315**, 160 (2011).

[15] Z. Bouchkour, P. Tristant, E. Thune, C. Dublanche-Tixier, C. Jaoul, and R. Guinebretiere, Surf. Coat. Technol. **205**, S586 (2011).

[16] K. S. Novoselov, A. K. Geim, S. V. Morozov, D. Jiang, M. I. Katsnelson, I. V. Grigorieva, S. V. Dubonos, and A. A. Firsov, Nature (London) **438**, 197 (2005).

[17] A. Kara, H. Enriquez, A. P. Seitsonen, L. C. L. Y. Voon, S. Vizzini, B. Aufray, and Hamid Oughaddou, Surf. Sci. Rep. **67**, 1 (2012).

[18] H. Liu, J. Gao, and J. Zhao, J. Phys. Chem. C **117**, 10353 (2013).

[19] H. Sahin, J. Sivek, S. Li, B. Partoens, and F. M. Peeters, Phys. Rev. B **88**, 045434 (2013).

[20] S. Cahangirov, M. Topsakal, E. Akturk, H. Sahin, and S. Ciraci, Phys. Rev. Lett. **102**, 236804 (2009).

[21] Z. Ni, Q. Liu, K. Tang, J. Zheng, J. Zhou, R. Q. Z. Gao, D. Yu, and J. Lu, Nano Lett. **12**, 113 (2012).

[22] M. E. Davila, L. Xian, S. Cahangirov, A. Rubio, and G. Le Lay, New J. Phys. **16**, 095002 (2014).

[23] K. Yang, S. Cahangirov, A. Cantarero, A. Rubio, and R. D'Agosta, Phys. Rev. B **89**, 125403 (2014).

[24] K. S. Novoselov, D. Jiang, F. Schedin, T. J. Booth, V. V. Khotkevich, S. V. Morozov, and A. K. Geim, Proc. Natl. Acad. Sci. (USA) **102**, 10451 (2005).

[25] R. A. Gordon, D. Yang, E. D. Crozier, D. T. Jiang, and R. F. Frindt, Phys. Rev. B **65**, 125407 (2002).

[26] J. N. Coleman, M. Lotya, A. O'Neill, S. D. Bergin, P. J. King, U. Khan, K. Young, A. Gaucher, S. De, R. J. Smith, I. V. Shvets, S. K. Arora, J. J. Boland, J. J. Wang, J. F. Donegan, J. C. Grunlan, G. Moriarty, A. Shmeliov, R. J. Nicholls, J. M. Perkins, E. M. Grieveson, K. Theuwissen, D. W. McComb, P. D. Nellist, and V. Nicolosi, Science **331**, 568 (2011).

[27] Q. H. Wang, K. Kalantar-Zadeh, A. Kis, J. N. Coleman, and M. S. Strano, Nat. Nanotech. **7**, 699 (2012).

[28] J. S. Ross, P. Klement, A. M. Jones, N. J. Ghimire, J. Yan, D. G. Mandrus, T. Taniguchi, K. Watanabe, K. Kitamura, W. Yao, D. H. Cobden, and X. Xu, Nat. Nanotech. **9**, 268 (2014).

[29] S. Tongay, J. Zhou, C. Ataca, K. Lo, T. S. Matthews, J. Li, J. C. Grossman, and J. Wu, Nano Lett. **12**, 5576 (2012).

[30] H. Sahin, S. Tongay, S. Horzum, W. Fan, J. Zhou, J. Li, J. Wu, and F. M. Peeters, Phys. Rev. B **87**, 165409 (2013).

[31] S. Tongay, H. Sahin, C. Ko, A. Luce, W. Fan, K. Liu, J. Zhou, Y.-S. Huang, C.-H. Ho, J. Yan, D. F. Ogletree, S. Aloni, J. Ji, S. Li, J. Li, F. M. Peeters, and J. Wu, Nat. Commun. **5**, 3252 (2014).

[32] H. L. Zhuang and R. G. Hennig, Appl. Phys. Lett. **101**, 153109 (2012).

[33] Q. Wang, Q. Sun, P. Jena, and Y. Kawazoe, ACS Nano **3**, 621 (2009).

[34] K. K. Kim, A. Hsu, X. Jia, S. M. Kim, Y. Shi, M. Hofmann, D. Nezich, J. F. Rodriguez-Nieva, M. Dresselhaus, T. Palacios, and J. Kong, Nano Lett. **12**, 161 (2012).

[35] M. Farahani, T. S. Ahmadi, and A. Seif, J. Mol. Struct. **913**, 126 (2009).

[36] H. Sahin, S. Cahangirov, M. Topsakal, E. Bekaroglu, E. Akturk, R. T. Senger, and S. Ciraci, Phys. Rev. B **80**, 155453 (2009).

[37] P. Tsipas, S. Kassavetis, D. Tsoutsou, E. Xenogiannopoulou, E. Golias, S. A. Giamini, C. Grazianetti, D. Chiappe, A. Molle, M. Fanciulli, and A. Dimoulas, Appl. Phys. Lett. **103**, 251605 (2013).

[38] X. J. Du, Z. Chen, J. Zhang, C. S. Yao, and C. Chen, Superlattices Microstruct. **52**, 662 (2012).

[39] F. L. Zheng, J. M. Zhang, Y. Zhang, and V. Ji, Physica B **405**, 3775 (2010).

[40] E. F. de Almeida Junior, F. de Brito Mota, C. M. C. de Castilho, A. Kakanakova-Georgieva, and G. K. Gueorguiev, Eur. Phys. J. B. **85**, 48 (2012).

[41] Q. Chen, R. Song, C. Chen, and X. Chen, Solid State Commun. **172**, 24 (2013).

[42] C. Shi, H. Qin, Y. Zhang, J. Hu, and L. Ju, J. Appl. Phys. **115**, 053907 (2014).

[43] G. Kresse and J. Hafner, Phys. Rev. B **47**, 558 (1993).

[44] G. Kresse and J. Hafner, Phys. Rev. B **49**, 14251 (1994).

[45] G. Kresse and J. Furthmüller, Comput. Mater. Sci. **6**, 15 (1996).

[46] G. Kresse and J. Furthmüller, Phys. Rev. B **54**, 11169 (1996).

[47] W. Kohn and L. J. Sham, Phys. Rev. **140**, A1133 (1965).

[48] J. P. Perdew, K. Burke, and M. Ernzerhof, Phys. Rev. Lett. **77**, 3865 (1996).

[49] J. P. Perdew, K. Burke, and M. Ernzerhof, Phys. Rev. Lett. **78**, 1396 (1997).

[50] J. Heyd, G. E. Scuseria, and M. Ernzerhof, J. Chem. Phys. **118**, 8207 (2003).

[51] S. J. Grimme, Comput. Chem. **27**, 1787 (2006).

[52] T. Bucko, J. Hafner, S. Lebegue, and J. G. Angyan, J. Phys. Chem. A **114**, 11814 (2010).

[53] G. Henkelman, A. Arnaldsson, and H. Jonsson, Comput. Mater. Sci. **36**, 354 (2006).

[54] C. L. Freeman, F. Claeyssens, N. L. Allan, and J. H. Harding, Phys. Rev Lett. **96**, 066102 (2006).
[55] Y. Baskin and L. Meyer, Phys. Rev. **100**, 544 (1955).
[56] D. Chung, J. Mater. Sci. **37**, 1475 (2002).
[57] W. Paszkowicz, J. B. Pelka, M. Knapp, T. Szyszko, and S. Podsiadlo, Appl. Phys. A **75**, 431 (2002).
[58] A. Marini, P. Garcia-Gonzalez, and A. Rubio, Phys. Rev. Lett. **96**, 136404 (2006).
[59] Y. Shi, C. Hamsen, X. Jia, K. K. Kim, A. Reina, M. Hofmann, A. L. Hsu, K. Zhang, H. Li, Z. Y. Juang, M. S. Dresselhaus, L. J. Li, and J. Kong, Nano Lett. **10**, 4134 (2010).
[60] D. Alfe, Comp. Phys. Commun. **180**, 2622 (2009).